RSC Advances

PAPER

View Article Online
View Journal | View Issue

Cite this: *RSC Adv.*, 2024, **14**, 24492

Hydrothermal liquefaction for biochar production from finger millet waste: its valorisation, process optimization, and characterization†

Afzal Hussain,‡[a] Ayush Kandari,‡[b] Sushant Kotiyal,[b] Vinod Kumar,[bcd] Shuchi Upadhyay,[e] Waseem Ahmad,[f] Ajay Singh[g] and Sanjay Kumar*[b]

In this study, the potential of finger millet waste biomass (FMWB) as a source of biochar production through hydrothermal liquefaction (HTL) was investigated. The HTL process was designed using Box–Behnken design (BBD) and carried out with process variables, *i.e.*, temperature (250 °C, 350 °C, and 450 °C), time (30 min, 45 min, and 60 min), and solid-to-water ratio (1 : 6, 1 : 8, and 1 : 10). The responses, *i.e.*, biochar yield (%), bulk density (g cm^{-3}), pH, and high heating value (HHV), were analysed. Optimisation was done using design expert software (version 13.0.1). The optimized finger millet waste biochar (O-F_MW_{BC}) was produced at optimum values (450 °C, 1 : 10, and 33.5 min). The results of proximate and elemental analysis revealed that moisture, ash, and volatile content, H, and O of O-F_MW_{BC} decreased while fixed carbon, thermal stability, and C content increased compared to FMWB. FT-IR, SEM-EDX, and XRD analyses were performed for O-F_MW_{BC}. The results of FT-IR showed the presence of O–H, C–H, C=O, and C=C functional groups. The SEM image revealed the rough surface of O-F_MW_{BC}, and XRD confirmed the production of a broad range of inorganic compounds and minerals. This study provides the full exploitation of F_MW_{BC} as a source of solid fuel.

Received 29th May 2024
Accepted 28th July 2024

DOI: 10.1039/d4ra03945a

rsc.li/rsc-advances

1 Introduction

Biomass, a renewable energy source, has been demonstrated to be one of the most environmentally friendly substitutes for fossil fuels.[1] Although fossil fuels are a good and convenient energy source, expanding their use not only accelerates the depletion of finite reserves of fossil fuels but also exacerbates air pollution and global climate change.[2] Consumption of resources such as coal, gas, and oil has expanded considerably in recent decades as global energy demand has increased.[3] The use of fossil fuels emits a large amount of greenhouse gases. Because of the issues associated with fossil fuels' usage, renewable energy sources have been created and implemented.[2,4] Biochar is a great fit for usage as a renewable fuel in the generation of power due to its high carbon and energy content.[5,6] The International Biochar Initiative[7] defines biochar as a carbon-containing solid generated by the thermochemical transformation of biomass in the absence of oxygen. Biochar adsorbs cations and ions from solution, as well as polar and non-polar chemical molecules.[8] Biochar is unquestionably a better fuel than raw biomass, having superior combustion characteristics and behaviour.[9–11]

Biomass holds significant promise as a potential source for biochar production, which can effectively address waste management. With the abundance and accessibility of agricultural byproducts, they prove to be ideal raw materials for biochar manufacturing and waste management, as highlighted by Sugumaran and Seshadri.[12] Every year, the production of waste biomass reaches a staggering 220 billion dry tonnes worldwide, making it the most significant and environmentally friendly source of biomass.[13] As the global demand for nutritious and sustainable crop options continues to rise due to increasing hunger, food insecurity, and challenges in our food systems, millets have become a top choice. Millets adapt themselves well to further processing into nutrient-rich functional goods that may be efficiently incorporated into our food supply due to their high nutritional content and resilience to climate change.[14,15] Unfortunately, byproducts of millet processing, such as leftovers from millet

[a]*Department of Pharmacognosy, College of Pharmacy, King Saud University, PO Box 2457, Riyadh 11451, Saudi Arabia*
[b]*Department of Food Science and Technology, Graphic Era (Deemed to be University), Dehradun, 248002, Uttarakhand, India. E-mail: mr.sanju4u@gmail.com*
[c]*Peoples' Friendship, University of Russia, (RUDN University), Moscow 117198, Russian Federation*
[d]*Graphic Era Hill University, Dehradun, 248002, Uttarakhand, India*
[e]*Department of Allied Health Sciences, School of Health Sciences and Technology, UPES, Dehradun, 248007, Uttarakhand, India*
[f]*Department of Chemistry, Graphic Era (Deemed to be University), Dehradun, 248002, Uttarakhand, India*
[g]*School of Applied and Life Sciences, Uttaranchal University, Dehradun, 248007, India*

† Electronic supplementary information (ESI) available. See DOI: https://doi.org/10.1039/d4ra03945a

‡ These authors contributed equally.

milk production, are often abandoned and wasted. Therefore, these byproducts may serve as a potential source for biochar production.

Rapidly increasing awareness of environmental issues and waste management challenges has led to increased interest in hydrothermal liquefaction (HTL) as the most evolving technology. This innovative approach is gaining popularity and offers a potential option to effectively convert waste into energy.[16–18] HTL significantly reduces the oxygen levels in biomass to approximately 10% of the biocrude through hydrolysis processes and improves conversion yields. High temperature, high pressure, dehydration, decarboxylation reactions, and longer reaction times are factors contributing to the success of this conversion process. Once the process is complete, four separate products are formed: an aqueous phase, a solid phase, a gas stream, and a bio-crude. These all depend on reaction factors such as temperature and duration. HTL is the most effective way to create a diverse range of products. For example, the solid product can be used to produce activated carbon-based compounds for both energy and environmental purposes.[19]

This research was prompted by the above-mentioned research findings, with the main objective of determining the feasibility of using finger millet waste as a source for biochar production that could serve as an alternative fuel source. Through a series of experiments, the waste was subjected to hydrothermal treatment, the main outcome of which was biochar production. A comprehensive analysis of the produced biochar was carried out using techniques such as FTIR, SEM-EDX, HHV analysis, particle size analysis, pH levels, bulk density, water holding capacity, and thermogravimetric analysis in order to thoroughly understand the properties of the biochar. Based on the results, the potential of the biochar produced in the current study as a solid substitute for conventional fuel sources was thoroughly investigated.

2 Materials and methods

2.1 Raw material and sample preparation

Finger millet was procured from the local market in Dehradun, India. Finger millet was steeped in water overnight. After that, millets were left overnight for germination. For the extraction of milk, millets were crushed with an equal amount of water in a household grinder. The mixture was then strained, and milk was collected. The finger millet waste biomass (**FMWB**) was dried at 50 °C in a tray dryer for 6–8 h. After drying, the FMWB was grinded in household mixer-grinder (Sujata Powermatic Plus 900 W, India) and stored in airtight containers for further processing and analysis.

2.2 Proximate analysis of raw material

The standard procedure of AOAC[20] was used to determine the moisture content (%) and ash content (%) of F_MW_B. Volatile matter (%) and fixed carbon (%) in the biomass were evaluated by the method outlined by Kumar *et al.*[21]

2.3 Elemental analysis

An elemental analyzer (Flash 2000 Series, Thermo Scientific) was used for the determination of C, H, and N content in F_MW_B. The amount of O content was calculated by the difference method. The high heating value, *i.e.*, HHV (MJ kg^{-1}) of F_MW_B and finger millet waste biochar (F_MW_{BC}), was calculated using the following equation (eqn (1)):

Table 1 Experimental data for biochar yield, pH, HHV and WHC of finger millet waste biochar (F_MW_{BC})[a]

	Independent variables			Responses			
Std	Temperature X_1	Time X_2	Solid-to-water ratio X_3	Biochar yield (%)	Bulk density (g cm^{-3})	pH	HHV (MJ kg^{-1})
1	250	30	8	36.6	0.1357	5.3	8.25
2	450	30	8	37.1**	0.1417	5.9**	27.71
3	250	60	8	36.9	0.1792	5.1	22.27
4	450	60	8	27.5	0.1025*	5.1	21.82
5	250	45	6	36.5	0.1388	5.2	9.2
6	450	45	6	22.4	0.1149	5.6	26.85
7	250	45	10	32.85	0.1366	5.4	22.92
8	450	45	10	29.3	0.1206	5.4	27.67**
9	350	30	6	33.5	0.1364	5.3	6.67
10	350	60	6	18.5*	0.173	5.9**	23.61
11	350	30	10	38	0.1231	5.7	15.49
12	350	60	10	32.8	0.1284	4.3*	26.04
13	350	45	8	29.67	0.2**	5.3	9.45
14	350	45	8	27.85	0.185	5.5	9.68
15	350	45	8	26.34	0.185	5.4	10.54
16	350	45	8	27.85	0.185	5.3	9.68
17	350	45	8	24.75	0.185	5.5	6.34*

[a] Represents minimum and maximum values, respectively. HHV means high heating value.

$$\text{HHV (MJ kg}^{-1}) = [0.3383\ C + 1.422\ \{H - (O/8)\}] \quad (1)$$

2.4 Experimental plan and model designing

Box–Behnken design (BBD) of response surface methodology (RSM) was used for the experimental plan to produce biochar and optimize the hydrothermal liquefaction (HTL) process variables to maximise the biochar yield and HHV and to minimise the bulk density of the produced F_MW_{BC}. A total of 17 experiments with 5 centre points were performed with 3 process variables (Table 1), *i.e.*, temperature (250 °C, 350 °C, 450 °C), time (30 min, 45 min, 60 min), and solid-to-water ratio (1 : 6, 1 : 8, 1 : 10), while biochar yield (%), bulk density (g cm^{-3}), pH, and HHV (MJ kg^{-1}) were analysed as response variables using Design Expert software. All the experimental data was fitted into the following second-order quadratic model equation (eqn (2)):

$$Y = \beta_0 + \sum_{i=1}^{n} \beta_i X_i + \sum_{i=1}^{n-1} \sum_{j=i+1}^{n} \beta_{ij} X_i X_j + \sum_{i=1}^{n} \beta_{ii} X_i^2 \quad (2)$$

where Y = response (biochar yield (%), bulk density (g cm^{-3}), pH, and HHV (MJ kg^{-1})), β_0, β_i, β_{ii} and β_{ij} are coefficients, and X_i and X_j denote process variables (where i = 1, 2, ……, n and

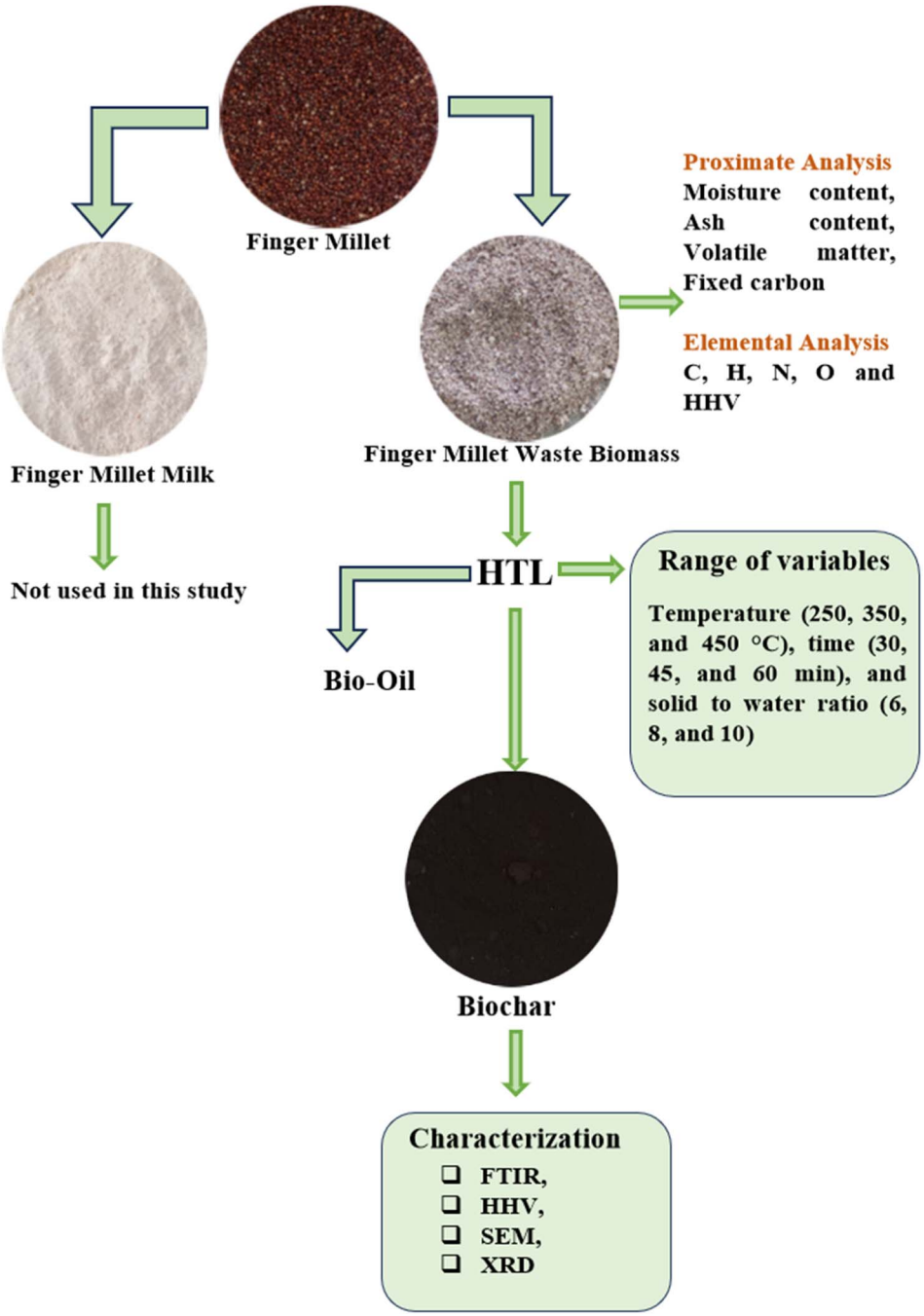

Fig. 1 Schematic illustration of present study.

$j = 1, 2, \ldots, n$). Fig. 1 represents the schematic illustration of the experimental plan for the present study.

2.5 Hydrothermal liquefaction (HTL) procedure

A custom-designed stainless steel (SS-316) reactor of 40 mL capacity was used to perform the HTL of F_MW_B. A muffle furnace was used to heat the reactor. Methodology of Hussain *et al.*[19] was adopted for the hydrothermal liquefaction procedure to produce F_MW_{BC}. All 17 designed experimental reactions were performed as per the combination of process variables given in Table 1. After the completion of the reaction, both the liquid and solid phases were collected separately using filtration. Dichloromethane was added in the liquid phase to recover the oil. The solid phase was washed 3–4 times with acetone. To obtain the biochar, the washed solid phase was dried in a hot air oven at 50 ± 5 °C for 3–4 h and weighed. For subsequent analysis, the dried F_MW_{BC} was kept at room temperature in an airtight container. The oil and gas produced were not considered in this study.

3 Biochar characterization

3.1 Biochar yield

The yield of F_MW_{BC} was determined using the equation given below (eqn (3)).

$$\text{Biochar yield } (\%) = \frac{W_{dbc}}{W_b} \times 100 \quad (3)$$

where, W_{dbc} and W_b represent the weights of dried biochar and biomass, respectively.

3.2 pH

The pH of F_MW_{BC} was analysed using a handy pH meter (Eutech pH 0.2). Briefly, in one part of F_MW_{BC}, two parts of deionized water were added and mixed. The pH was then recorded at room temperature.

3.3 Bulk density

Methodology of Askeland *et al.*[22] was adopted to access the bulk density of biochar. Bulk density of biochar was performed by filling a 50 mL graduated cylinder with 5 g of biochar sample. The volume of the 5 g sample was measured, and the bulk density was calculated using the following equation (eqn (4)) and expressed in g cm^{-3}.

$$\text{Bulk density(BD)} = \frac{M_{bc}}{V_{bc}} \quad (4)$$

where $M_{bc}$and V_{bc} are the mass and volume of biochar.

4 Characterization of F_MW_{BC}

4.1 FT-IR

To identify the functional group in F_MW_{BC}, a FT-IR spectrophotometer (PerkinElmer) was used. Briefly, in powdered F_MW_{BC}, potassium bromide powder (KBr) was added, and the mixture was then pulverized under high pressure to prepare pellets.[22] The FT-IR analysis of F_MW_{BC} was measured between 500 and 4000 cm^{-1}.

4.2 SEM analysis

Scanning electron microscope (ZEISS, EVO18) was used to examine the structural morphology of F_MW_{BC}.

4.3 X-ray diffraction spectra analysis

The XRD (Rigaku X-ray diffractometer) pattern of F_MW_{BC} was used to analyse phase evaluations as well as structural characteristics such as crystallinity. The diffraction angle range in the present study was 10° to 80°, and the scanning rate was 20/min.

4.4 Statistical analysis

The Design Expert Software (version 13.0.1) was used for numerical optimization of the experimental data in this study. The standard deviation, mean, % C.V. (coefficient of variance), coefficient (R^2), adjusted coefficient (adj. R^2) of determination, *F*-values, *p*-values, and lack of fit acquired for ANOVA to determine the effects of significant ($p < 0.05$) interactions in the model were used to assess the potency of the second order quadratic model equation eqn (2). A good adequate precision value greater than 4 also indicates a suitable signal-to-noise ratio.[23,24] The diagnostic tools included in the software contributed to the model's ability to predict responses. The results were validated using the second order quadratic model with optimized parameters. Using eqn (5), the (%) error was calculated to estimate the fit of the quadratic model.

$$\text{Error}(\%) = \frac{(\text{Experimental value} - \text{predicted value})}{\text{Experimental value}} \times 100 \quad (5)$$

The tests were conducted out in triplets for physicochemical analysis, and the findings were reported as mean ± SD.

Table 2 Results of proximate and elemental analysis of finger millet waste biomass (F_MW_B) and biochar (F_MW_{BC})

Parameters	F_MW_B	F_MW_{BC}
Proximate analysis		
Moisture content[a] (%)	14.3	5.1
Ash content[a] (%)	2.0	1.56
Volatile matter[a] (%)	13.93	0.62
Fixed carbon[a] (%)	69.77	92.72
Thermal stability	0.8335	0.993
Elemental analysis		
C	68.63	71.75
H	5.31	4.87
N	3.81	4.32
O[b]	22.25	18.06
HHV (MJ kg^{-1})	26.81	28.32

[a] Represents value on % dry basis. [b] Calculate by difference method, HHV: high heating value.

5 Results and discussion

5.1 Proximate and elemental analysis of finger millet waste (F_MW_B)

Table 2 displays the results of the proximate and elemental analysis of F_MW_B and O-F_MW_{BC}. The results show a reduction in moisture content, ash content, and volatile content of O-F_MW_{BC} owing to the thermal decomposition and degradation of non-carbon components, cellulose, hemicellulose, and lignin, *via* a hydrothermal liquefaction process at 450 °C.[25] These findings are consistent with the findings of Chen *et al.*[26]

The fixed carbon content of O-F_MW_{BC} increased 24.75% with respect to F_MW_B. The fixed carbon content, *i.e.*, 92.77 of O-F_MW_{BC}, is higher than those of *Camellia oleifera* shells hydrochar,[26] and *Ricinus communis* biochar.[27] The thermal stability of O-F_MW_{BC} increased 16.06% with respect to F_MW_B. The increase in thermal stability of O-F_MW_{BC} could be attributed to the high temperature (450 °C) of the hydrothermal liquefaction process, increase in fixed carbon, and decrease in volatile matter.[28] From the elemental analysis of F_MW_B and O-F_MW_{BC}, it was observed that H and O content of O-F_MW_{BC} decreased while the C and HHV content of O-F_MW_{BC} increased due to the hydrothermal liquefaction process at 450 °C. The increase in C content could be due to the decarboxylation, dehydration, and hydrolysis of F_MW_B.[29]

5.2 Model fitting and analysis of variance

This study explored and evaluated the impact of process variables *i.e.*, temperature (250 °C, 350 °C, 450 °C), duration (30 min, 45 min, 60 min), and solid-to-water ratio (1 : 6, 1 : 8, 1 : 10) on biochar yield (%), bulk density (g cm^{-3}), pH, and HHV (MJ kg^{-1}). Table 2 depicts the experimental results of biochar yield (%), bulk density (g cm^{-3}), pH, and HHV (MJ kg^{-1}). The maximum (37.1%) and minimum (18.5%) biochar yield were achieved in experiment no. 2 (450 °C, 30 min, 1 : 8) and experiment no. 10 (350 °C, 60 min, 1 : 6). The highest bulk density (0.2 g cm^{-3}) was observed in experiment no. 13 (350 °C, 45 min, 1 : 8), while the minimum value (0.1025 g/cm^3) was observed in experiment no. 4 (450 °C, 60 min, 1 : 8). The maximum (5.9) and minimum (4.3) pH of F_MW_{BC} was noted in experiment no. 2 (450 °C, 30 min, 1 : 8), experiment no. 10 (350 °C, 60 min, 1 : 6), and experiment no. 12 (350 °C, 60 min, 1 : 10), respectively. The HHV of F_MW_{BC} was observed to be maximum (27.67 MJ kg^{-1}) and minimum (6.34 MJ kg^{-1}) in experiment no. 8 (450 °C,

Table 3 ANOVA of experimental responses[a]

	Biochar yield (%)		Bulk density (g cm^{-3})		pH		HHV (MJ kg^{-1})	
Factor	*F*-value	*p*-value	*F*-value	*p*-value	*F*-value	*p*-value	*F*-value	*p*-value
Model	5.13	0.0212	11.60	0.0019	6.32	0.0119	13.47	0.0012
X_1	9.03	0.0198*	11.31	0.0120*	3.80	0.0921**	24.96	0.0016*
X_2	11.15	0.0124*	1.97	0.2029	12.33	0.0098*	18.47	0.0036*
X_3	6.23	0.0412*	2.74	0.1421	5.48	0.0518**	9.68	0.0170*
X_1X_2	2.51	0.1570	12.64	0.0093*	2.74	0.1419	11.54	0.0115*
X_1X_3	2.85	0.1351	0.1154	0.7441	1.22	0.3064	4.84	0.0636**
X_2X_3	2.46	0.1607	1.81	0.2203	30.43	0.0009*	1.19	0.3117
X_1^2	4.98	0.0608**	28.71	0.0011*	0.0801	0.7854	26.06	0.0014
X_2^2	6.35	0.0398*	9.94	0.0161*	0.7208	0.4240	6.30	0.0405*
X_3^2	0.0788	0.7871	27.86	0.0012*	0.0801	0.7854	13.41	0.0080*
Lack of fit	5.34	0.0697	5.68	0.0633	6.33	0.0533	6.32	0.0535*
R^2	0.8684		0.9372		0.8904		0.9454	
Adjusted R^2	0.6992		0.8564		0.7495		0.8753	
Std. dev	3.12		0.0116		0.1813		2.93	
Mean	30.49		0.1512		5.36		16.72	
C.V. %	10.24		7.69		3.38		17.53	
Adequate precision	7.30		8.84		10.43		9.53	

[a] Represents $p < 0.05$, and $0.05 \leq p < 0.1$, respectively; no superscript $= p \geq 0$.

Table 4 Constraints for optimization of process parameters, predicted and experimental values of responses

Variables	Goal	Lower level	Upper level	Optimized values/predicted values	Experimental values	Error (%)
X_1: temperature (°C)	In range	250	450	450	450	—
X_2: time (min)	In range	30	60	33.53	33.5	—
X_3: solid to water ratio	In range	6	10	10	10	—
Biochar yield (%)	Maximize	18.5	38	37.41	38.38 ± 0.19	2.52
Bulk density (g cm^{-3})	Minimize	0.1025	0.2	0.11	0.12 ± 0.08	8.3
pH	In range	4.3	5.9	5.9	5.6 ± 0.11	−5.35
HHV (MJ kg^{-1})	Maximize	6.34	27.71	30.55	28.32 ± 0.05	−7.29

45 min, 1 : 10) and experiment no. 17 (350 °C, 45 min, 1 : 8), respectively. The second-order quadratic model-based polynomial regression equations by eliminating insignificant coefficients for biochar yield, bulk density, pH, and HHV are illustrated as eqn (7)–(10).

$$\text{Biochar yield (\%)} = 27.292 - 3.318\ X_1 - 3.687\ X_2 + 2.756\ X_3 + 3.835\ X_2^2 \quad (7)$$

$$\text{Bulk density (g cm}^{-3}) = 0.188 - 0.013\ X_1 - 0.020\ X_1\ X_2 - 0.030\ X_1^2 - 0.017\ X_2^2 - 0.029\ X_3^2 \quad (8)$$

$$\text{pH} = 5.4 - 0.225\ X_2 - 0.5\ X_2\ X_3 \quad (9)$$

$$\text{HHV (MJ kg}^{-1}) = 9.138 + 5.176\ X_1 + 4.452\ X_2 + 3.223\ X_3 - 4.977\ X_1\ X_2 + 7.291\ X_2^2 + 3.583\ X_2^2 + 5.321\ X_3^2 \quad (10)$$

In eqn (7)–(10), positive and negative signs showed that process variables can enhance and lower the responses, respectively. A negative sign at the linear level suggests a decrease in response when level of predictor level is increased, whereas increase in response is shown by a positive sign. For a constant response

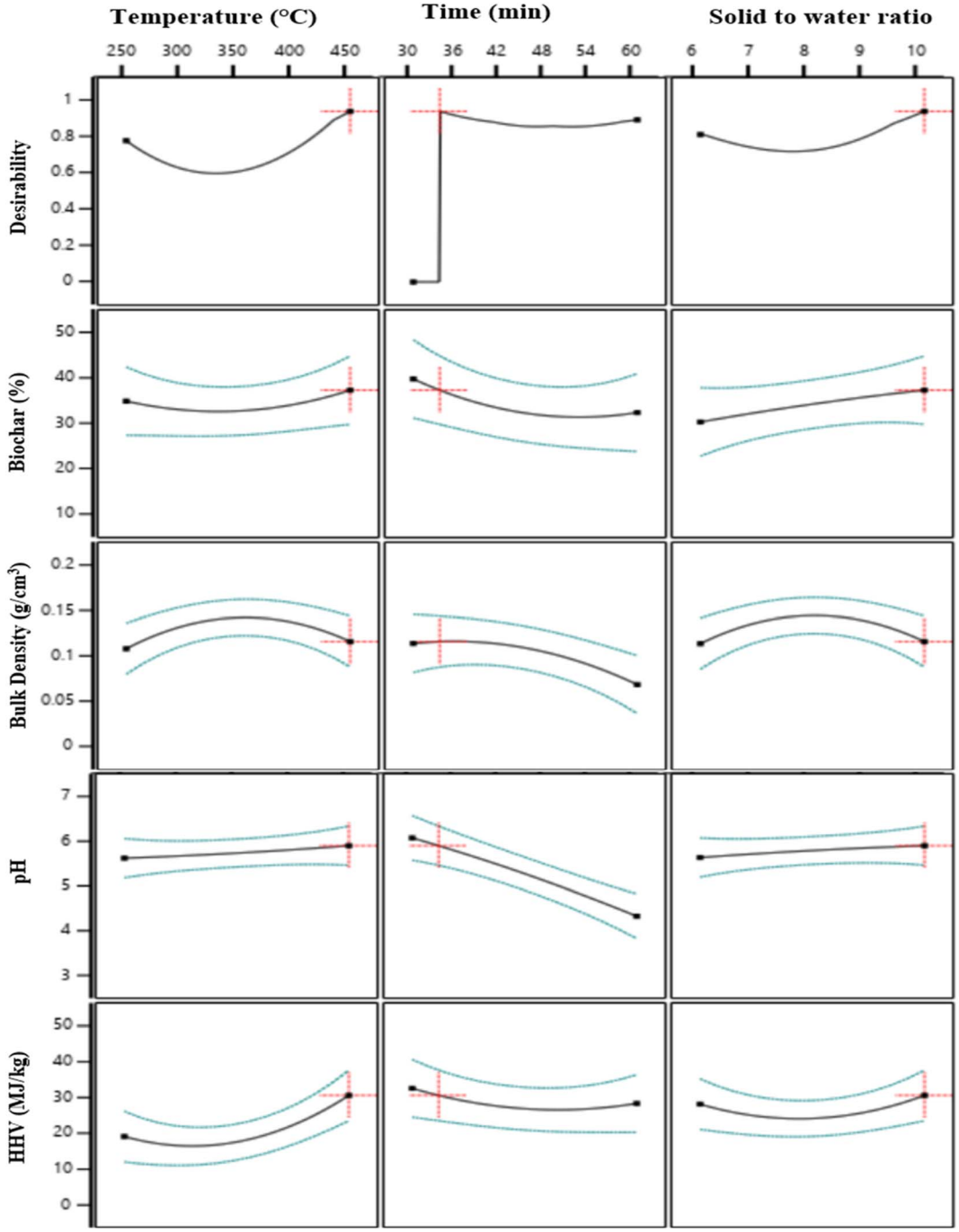

Fig. 2 Response optimization for O-$F_M W_{BC}$.

value, a significant negative interaction implies that there can be increase in the level of one predicted variable while there is decrease in the level of other. Positive interaction indicates minimal reaction at the centre point and an increase in the reaction as both variables deviate from the centre point. Minimal reaction at the centre value of the parameter is shown by the positive coefficient of the quadratic term, and it rises with an increase or decrease in the parameter level. The greatest reaction at the centre value that diminishes with an increase or decrease in parameter level is exhibited by the negative coefficient of the quadratic term.

For model fitting and data validation, the analysis of variance was computed using Design Expert software and tabulated in Table 3. The *F*-values for biochar yield, bulk density, pH, and HHV were predicted to be 5.13, 11.60, 6.32, and 13.47, respectively, implying that the second-order quadratic model is significant and that the large *F*-values are only 2.12%, 0.19%, 1.19%, 0.12%, and 0.20% likely to be due to noise. *P*-values were less than 0.05 for biochar yield (0.0212), bulk density (0.0019), pH (0.0119), and HHV (0.0012), suggesting that the response models are significant (Table 3). Adequate precision values for biochar yield (7.30), bulk density (8.84), pH (10.43), and HHV (9.53) were higher than 4.0, indicating an adequate signal, and these second-order quadratic models can be used to navigate the design space. The coefficient of variation (% C.V.) for biochar yield, bulk density, pH, and HHV, respectively, was 10.24, 7.69, 3.38, and 17.53, indicating the least variation in experimental data suited to the second order quadratic model due to higher mean values of 30.49, 0.1512, 5.36, and 16.72 for biochar yield, bulk density, pH, and HHV, respectively. A lower lack of fit compared to F-values for biochar yield, bulk density, pH, and HHV reveals an insignificant lack of fit. The diagnostics plots *i.e.* normal probability and externally studentized residuals plots are given in Fig. S1 and S2.†

6 Product responses

6.1 Biochar yield

According to Ponnusamy *et al.*,[30] the biochar yield is determined by the thermochemical process used. Biochar yield increased when the HTL process temperature increased from 250 °C to 450 °C (Fig. S3(a) and (b)†), and a similar trend was observed as the solid-to-water ratio increased from 1 : 6 to 1 : 10 (Fig. S3(b) and (c)†). Selvarajoo *et al.*[1] also observed increase in biochar yield from 1.72 to 27.26 (% wt) when temperature increased from 300 to 500 °C. Jayathilake *et al.*[31] observed increase in biochar yield from 12% to 34% as the temperature increase from 573 K to 603 K. Biochar yield dropped as time rose from 30 to 60 minutes, as shown in Fig. S3(a) and (c).† Hussain *et al.*[19] also observed a decreasing trends of biochar yield as the time increases. The findings of this study confirm the concept that at high temperatures, biochar production increases owing to repolymerization, rearrangement reactions, and the development of char-like structures due to bonding between free radicals and other carbon atoms.[32–34]

6.2 Bulk density

Inter-particle voids and macro porosity within every particle of the raw material affect the bulk density of biochar.[8] Biochar with a bulk density of less than 1 g cm^{-3} has a significant role in its movement into the soil and enhanced soil aeration, porosity, and microbial respiration.[22,35,36]

The influence of process variables on bulk density is depicted in Fig. S4.† The bulk density of biochar increased with increasing temperature (250 to 450 °C), duration (30 min to 60 min), and solid to solvent ratio (1 : 6 to 1 : 10), as shown in Fig. S4(a–c).† This study's findings are consistent with the findings of Das *et al.*[36] The increased bulk density trends with increasing temperature might be attributed to an increase in the concentration of condensed aromatic compounds in the sample volume and a decrease in void space.[37]

6. 3pH

The pH affects the adsorption potential and nature of the active adsorbent centre on the surface of biochar.[38] The pH of biochar is also determined by its ash content, metal content, and manufacturing process.[39] pH varies from acidic, neutral to alkaline, acidic to alkaline, and neutral, based on the production process such as hydrothermal carbonization, gasification, slow pyrolysis, and rapid pyrolysis, respectively.[40–43] The pH value of F_MW_{BC} produced through hydrothermal liquefaction in the present study is low as it ranges from 4.3 to 5.9. Fig. S5(a) and S5(b),† depict that pH increased with increasing temperature. The value of pH also increased with increasing the solid-to-water ratio (Fig. S5(b) and S5(c)†). Whereas Fig. S5(a) and S5(b)† represents the decreasing trends of pH with increasing time.

6.4 HHV

The higher heating value (HHV) is an important statistic for determining the potential energy content of different biomass sources.[44] The higher heating value (HHV) of a fuel is the amount

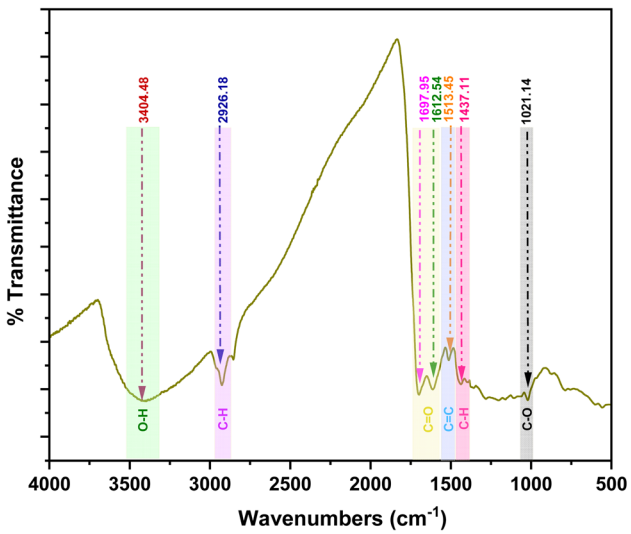

Fig. 3 FTIR spectra of O-F_MW_{BC}.

of heat produced when a unit quantity of fuel is entirely burnt, which includes the latent heat of vaporisation of water vapour produced when the fuel is burned. Higher HHV fuel gives a higher energy output.[45] The impact of temperature, time, and solid-to-water ratio on HHV can be predicted from Fig. S6(a–c).† In this study, increasing trends of HHV were observed as HTL process temperature (Fig. S6(a) and (b)†), time (Fig. S6(a) and (c)†), and solid-to-water ratio (Fig. S6(b) and (c)†) increased. Park *et al.*[45] observed an increase in HHV of spent coffee ground with temperature and time of HTC process. Selvarajoo and Oochit[46] also observed that when the pyrolysis temperature climbed from 300 to 700 °C, the HHV of palm fibre biochar increased by 16.088%. It might be due to the rise in temperature causing a decrease in oxygen concentration and an increase in carbon content in biochar. In another study conducted by Ahn *et al.*,[47] they concluded that the HHV of food waste biochar increased with increasing temperature and time. The increased HHV could be attributed to the release of ionic substances into the biochar and enhanced carbon content in biochar.[48,49]

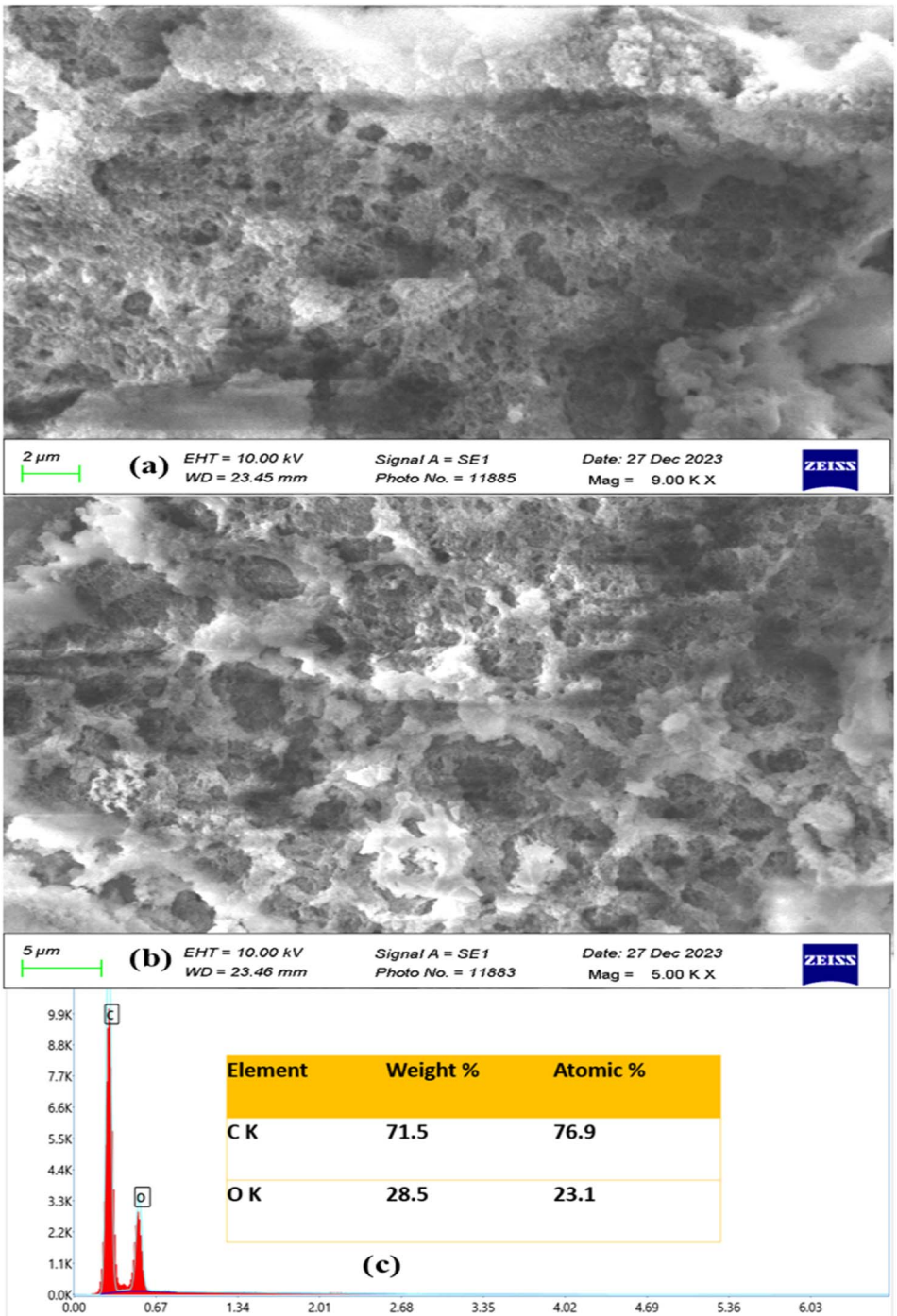

Element	Weight %	Atomic %
C K	71.5	76.9
O K	28.5	23.1

Fig. 4 SEM image of O-F_MW_{BC} at (a) 2 µm, (b) 5 µm, (c) elemental composition.

6.5 Numerical optimization and verification

Numerical optimization is a process of making compromises between responses, to achieve a common target. The goal was to maximise biochar yield and HHV, while minimising bulk density and keeping pH within a certain range (Table 4). The optimisation was performed using the criteria listed in Table 4. Several solutions were obtained during optimisation, and the one that best fit the criteria was chosen with the highest desirability *i.e.* 0.942 (Fig. 2). In Fig. 2 average value of results are presented by black lines, the upper and lower values of results are expressed by blue dote while the optimized value of corresponding response is described by red lines. The optimal conditions for producing biochar using the HTL process have been found to be 450 °C temperature, 33.53 min duration, and a solid-to-water ratio of 1 : 10. F_MW_{BC} was developed at optimal values to evaluate and verify the model, and the results are shown in Table 4. The experimental values of the responses of optimised F_MW_{BC} (O-F_MW_{BC}) are in agreement with the expected values with a small percentage of error (Table 4). The O-F_MW_{BC} produced at optimum conditions had biochar yield (38.38%), bulk density (0.12 g cm^{-3}), pH (5.6), and HHV (28.32 MJ kg^{-1}).

7 Characterization of O-F_MW_{BC}

7.1 FTIR analysis

The FTIR spectra of O-F_MW_{BC} is depicted in Fig. 3. Several peaks were observed at different wavelengths. A peak at 3404.48 cm^{-1} and 2926.18 cm^{-1} were correlated with O–H stretching and C–H vibrations.[50] The peak between 1612.54 cm^{-1} and 1697.95 cm^{-1} corresponds to C=O stretching, which confirms the formation of aromatic compounds, ketones, and carboxyl compounds.[51,52] The peak at 1513 cm^{-1} falls between 1610 cm^{-1} and 1510 cm^{-1} which represents the C=C stretching of hemicellulose.[53] The peaks 1437 cm^{-1} and 1021 cm^{-1} lies between 1480 cm^{-1} to 1410 cm^{-1} and 1120 cm^{-1} and 1050 cm^{-1} which confirms the C–H deformation and C–O stretching vibrations in hemicellulose and cellulose.[54]

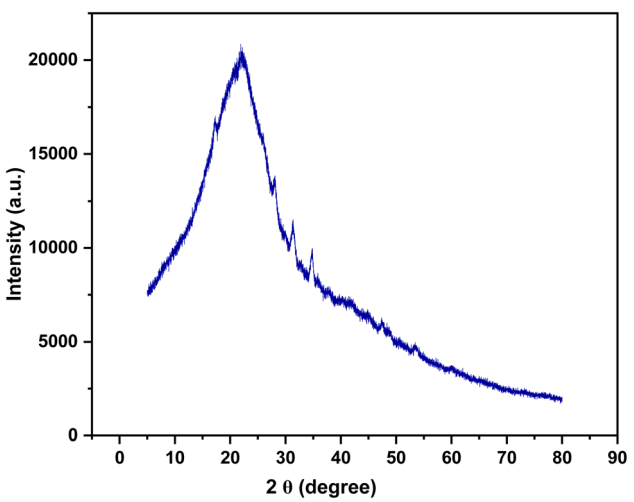

Fig. 5 XRD spectra of O-F_MW_{BC}.

7.2 SEM-EDX analysis

Scanning electron microscope images of the O-F_MW_{BC} at 2 μm and 5 μm are shown in Fig. 4(a–c) represents the elemental composition of O-F_MW_{BC}. The EDX results revealed the presence of carbon (71.5%) and oxygen (28.5%) as predominant components. The surface morphology of the developed biochar was illustrated in Fig. 4(a) and (b). The surface structure of the developed biochar shows a subtle porosity. The porous surface of the biochar may be attributed to the volatilization of the organic components. The organic components present in the biochar become volatile during the thermal treatment leading to the formation of the porous surface of the biochar. Releasing the volatile material subsequently enhanced the surface area of the developed biochar. Nevertheless, a small fraction of the developed biochar showed smaller particles with the textured surface. The biochar also showed some flake like structure due to the filling of micro pores with the volatile organic material and their other decomposition product.

7.3 XRD analysis

The XRD spectra of O-F_MW_{BC} is shown in Fig. 5. The various peaks at 21.29°, 28.14°, 31.41°, 47.55°, 53.24°, and 59.93° in the XRD spectra of O-F_MW_{BC} confirm the production of a broad range of inorganic compounds and minerals. The strong peak at 2θ = 21.92° corresponding to plane (001) indicates the amorphous nature of the O-F_MW_{BC}. Another peak at 2θ = 28.17° and 31.41° confirms the formation of fluorite and chlorapatite in O-F_MW_{BC}. The peaks in the range of 53.24°–59.93° confirm the presence of quartz and Ca silicates, Mg silicates, and Mn silicates.

8 Conclusion

The HTL process was designed using Box–Behnken design (BBD) and carried out with process variables *i.e.* temperature (250 °C, 350 °C, and 450 °C), time (30 min, 45 min, and 60 min), and solid to water ratio (1 : 6,1 : 8, and 1 : 10). The responses *i.e.*, biochar yield (%), bulk density (g cm^{-3}), pH, and high heating value (HHV) were analysed. The O-F_MW_{BC} was produced at 450 °C temperature, 1 : 10 solid to water ratio, and 33.5 min. The findings indicated that HHV and C content increased, and O and H content decreased when HTL process is carried out at 450 °C. FT-IR confirmed the presence of O–H, C–H, C=O, and C=C functional groups while XRD confirm the formation of fluorite, chlorapatite, quartz and Ca silicates, Mg silicates and Mn silicates in O-F_MW_{BC}. In conclusion, further study is required to utilize the O-F_MW_{BC} into the agriculture system which could open new path to remove the pollutants from water, and soil for sustainable agriculture. The use of biochar into agricultural systems presents a significant opportunity to tackle current issues related to crop yield, soil management, and environmental sustainability.

Data availability

Data will be made available on request.

Author contributions

All authors contributed to the study conception and design. Investigation and project administration was carried out by Sanjay Kumar. Conceptualization and supervision was carried out by Sanjay Kumar and Vinod Kumar. Methodology was carried out by Ayush Kandari and Sushant Kotiyal. The first draft of the manuscript was written by Afzal Hussain. Formal analysis were performed by Shuchi Upadhyay. Review and editing were performed by Ajay Singh, Waseem Ahmad. All authors read and approved the final manuscript.

Conflicts of interest

The authors declare that they have no competing interests.

Acknowledgements

The authors are grateful to the Department of Food Science & Technology, Graphic Era (Deemed to be University), Dehradun, Uttarakhand, India, for providing the necessary infrastructure for this research work. This paper has been supported by the RUDN University Strategic Academic Leadership Program. The authors acknowledge the generous support from the researchers supporting project number (RSPD2024R980) King Saud University, Riyadh, Saudi Arabia.

References

1 A. Selvarajoo, Y. L. Wong, K. S. Khoo, W. H. Chen and P. L. Show, *Chemosphere*, 2022, **294**, 133671.
2 L. Zhu, H. Lei, Y. Zhang, X. Zhang, Q. Bu and Y. Wei, *SF J. Mater. Chem. Eng.*, 2018, **1**(1), 1007.
3 P. L. C. BP, *Statistical Review of World Energy*, London, UK, 2020.
4 X. Yang, H. Wang, P. J. Strong, S. Xu, S. Liu, K. Lu, K. Sheng, J. Guo, L. He, Y. S. OK, G. Yuan, Y. Shen and X. Chen, *Energies*, 2017, **10**(4), 469.
5 Y. Lee, J. Park, C. Ryu, K. S. Gang, W. Yang, Y. K. Park, J. Jung and S. Hyun, *Bioresour. Technol.*, 2013, **148**, 196–201.
6 M. Tripathi, J. N. Sahu and P. Ganesan, *Renewable Sustainable Energy Rev.*, 2016, **55**, 467–481.
7 International Biochar Initiative, *Standardized Product Definition and Product Testing Guidelines for Biochar that Is Used in Soil*, IBI biochar standards. Victor: International Biochar Initiative, 2013.
8 G. Stella Mary, P. Sugumaran, S. Niveditha, B. Ramalakshmi, P. Ravichandran and S. Seshadri, *Int. J. Recycl. Org. Waste Agric.*, 2016, **5**, 43–53.
9 H. Abdullah and H. Wu, *Energy Fuels*, 2009, **23**(8), 4174–4181.
10 Z. Liu, A. Quek, S. K. Hoekman and R. Balasubramanian, *Fuel*, 2013, **103**, 943–949.
11 Z. Liu and G. Han, *Fuel*, 2015, **158**, 159–165.
12 P. Sugumaran and S. Seshadri, *J. Sci. Ind. Res.*, 2009, **68**(8), 719–723.
13 R. Azargohar, K. L. Jacobson, E. E. Powell and A. K. Dalai, *J. Anal. Appl. Pyrolysis*, 2013, **104**, 330–340.
14 A. Kumar, V. Tomer, A. Kaur, V. Kumar and K. Gupta, *Agric. Food Secur.*, 2018, **7**(1), 1–15.
15 M. Nani and K. Krishnaswamy, *Sci. Rep.*, 2023, **13**(1), 6482.
16 I. Fonts, G. Gea, M. Azuara, J. Ábrego and J. Arauzo, *Renewable Sustainable Energy Rev.*, 2012, **16**(5), 2781–2805.
17 M. Pham, L. Schideman, J. Scott, N. Rajagopalan and M. J. Plewa, *Environ. Sci. Technol.*, 2013, **47**(4), 2131–2138.
18 B. Bisht, P. Gururani, S. Pandey, K. K. Jaiswal, S. Kumar, M. S. Vlaskin, M. Verma, H. Kim and V. Kumar, *Fuel*, 2022, **328**, 125253.
19 A. Hussain, S. Kumar, F. M. Husain, V. Kumar, M. S. Vlaskin and M. F. Alajmi, *Environ. Sci. Pollut. Res.*, 2023, **30**(46), 102462–102473.
20 A. O. A. C., *Official Methods of Analysis of the Association of Official Analytical Chemists*, edn 17, 2000.
21 V. Kumar, K. K. Jaiswal, M. S. Vlaskin, M. Nanda, M. K. Tripathi, P. Gururani, S. Kumar and H. C. Joshi, *Biofuels*, 2022, **13**(5), 657–662.
22 M. Askeland, B. Clarke and J. Paz-Ferreiro, *PeerJ*, 2019, **7**, e6784.
23 S. Arora, P. Kataria, W. Ahmad, R. Mishra, S. Upadhyay, A. Dobhal, B. Bisht, A. Hussain, V. Kumar and S. Kumar, *Food Anal. Methods*, 2023, **17**, 105–118.
24 S. Mariyam, M. Alherbawi, S. Pradhan, T. Al-Ansari and G. McKay, *Biomass Convers. Biorefin.*, 2023, DOI: **10.1007/s13399-023-03825-6**.
25 C. Hadey, M. Allouch, M. Alami, F. Boukhlifi and I. Loulidi, *Sci. World J.*, 2022, **1**, 2554475.
26 C. Chen, W. Liang, F. Fan and C. Wang, *ACS Omega*, 2021, **6**(25), 16546–16552.
27 F. C. Luz, M. Volpe, C. Chiaruzzi, A. Picone and A. Messineo, *Chem. Eng. Trans.*, 2023, **98**, 117–122.
28 S. Masoumi, V. B. Borugadda, S. Nanda and A. K. Dalai, *Catalysts*, 2021, **11**(8), 939.
29 P. Gao, Y. Zhou, F. Meng, Y. Zhang, Z. Liu, W. Zhang and G. Xue, *Energy*, 2016, **97**, 238–245.
30 V. K. Ponnusamy, S. Nagappan, R. R. Bhosale, C. H. Lay, D. D. Nguyen, A. Pugazhendhi, S. W. Chang and G. Kumar, *Bioresour. Technol.*, 2020, **310**, 123414.
31 M. Jayathilake, S. Rudra, N. Akhtar and A. A. Christy, *Materials*, 2021, **14**(11), 3024.
32 B. Zhang, H. J. Huang and S. Ramaswamy, *Appl. Biochem. Biotechnol.*, 2008, **147**, 119–131.
33 T. L. K. Yong and Y. Matsumura, *Ind. Eng. Chem. Res.*, 2013, **52**, 5626–5639.
34 E. I. Kozliak, A. Kubátová, A. A. Artemyeva, E. Nagel, C. Zhang, R. B. Rajappagowda and A. L. Smirnova, *ACS Sustain. Chem. Eng.*, 2016, **4**, 5106–5122.
35 C. E. Brewer, V. J. Chuang, C. A. Masiello, H. Gonnermann, X. Gao, B. Dugan, L. E. Driver, P. Panzacchi, K. Zygourakis and C. A. Davies, *Biomass Bioenergy*, 2014, **66**, 176–185.
36 S. K. Das, G. K. Ghosh, R. K. Avasthe and K. Sinha, *J. Environ. Manage.*, 2021, **278**, 111501.
37 M. A. M. Salleh, D. K. Mahmoud, W. A. W. A. Karim and A. Idris, *Desalination*, 2011, **280**(1–3), 1–13.
38 S. M. Griffith, G. M. Banowetz and D. Gady, *Chemosphere*, 2013, **92**(10), 1275–1279.

39 K. Wiedner, C. Rumpel, C. Steiner, A. Pozzi, R. Maas and B. Glaser, *Biomass Bioenergy*, 2013, **59**, 264–278.
40 V. Hansen, D. Müller-Stöver, J. Ahrenfeldt, J. K. Holm, U. B. Henriksen and H. Hauggaard- Nielsen, *Biomass Bioenergy*, 2015, **72**, 300–308.
41 X. Y. Yu, G. G. Ying and R. S. Kookana, *Chemosphere*, 2009, **76**(5), 665–671.
42 S. Shackley, S. Carter, T. Knowles, E. Middelink, S. Haefele, S. Sohi, A. Cross and S. Haszeldine, *Energy Policy*, 2012, **42**, 49–58.
43 L. C. Malucelli, G. F. Silvestre, J. Carneiro, E. C. Vasconcelos, M. Guiotoku, C. M. B. F. Maia and M. A. S. Carvalho Filho, *J. Therm. Anal. Calorim.*, 2020, **139**, 2215–2220.
44 L. Xu and J. Yuan, *Fuel*, 2015, **161**, 68–77.
45 J. E. Park, G. B. Lee, C. J. Jeong, H. Kim and C. G. Kim, *Energies*, 2021, **14**(20), 6551.
46 A. Selvarajoo and D. Oochit, *Mater. Sci. Energy Technol.*, 2020, **3**, 575–583.
47 K. H. Ahn, D. C. Shin, Y. E. Lee, Y. Jeong, J. Jung and I. T. Kim, *Molecules*, 2023, **28**(16), 6114.
48 M. Wilk, A. Magdziarz and I. Kalemba, *Energy*, 2015, **87**, 259–269.
49 T. I. K Mathabatha, A. N. Matheri and M. Belaid, *Circ. Econ. Sustainability*, 2023, **3**, 1045–1064.
50 J. Chen and S. Li, *RSC Adv.*, 2020, **10**(4), 2160–2169.
51 Z. Liu, W. Niu, H. Chu, T. Zhou and Z. Niu, *BioResources*, 2018, **13**(2), 3429–3446.
52 A. Y. Elnour, A. A. Alghyamah, H. M. Shaikh, A. M. Poulose, S. M. Al-Zahrani, A. Anis and M. I. Al-Wabel, *Appl. Sci.*, 2019, **9**(6), 1149.
53 H. Yang, R. Yan, H. Chen, D. H. Lee and C. Zheng, *Fuel*, 2007, **86**(12–13), 1781–1788.
54 M. S. Reza, S. Afroze, M. S. Bakar, R. Saidur, N. Aslfattahi, J. Taweekun and A. K. Azad, *Biochar*, 2020, **2**, 239–251.